Molecular Crystals and Liquid Crystals

Publication details, including instructions for authors and subscription information:
http://www.tandfonline.com/loi/gmcl20

H-PDLC/Clay Nanocomposites

Yuan-Pin Huang [a], Yun-Min Chang [b], Tsung-Yen Tsai [b] & Wei Lee [c]

[a] Department of Chemical & Materials Engineering, Cheng Shiu University, Kaohsiung, Taiwan, Republic of China

[b] Department of Chemistry and Center for Nano-Technology, Chung Yuan Christian University, Chung-Li, Taiwan, Republic of China

[c] Department of Physics and Center for Nano-Technology, Chung Yuan Christian University, Chung-Li, Taiwan, Republic of China

Version of record first published: 05 Oct 2009

To cite this article: Yuan-Pin Huang, Yun-Min Chang, Tsung-Yen Tsai & Wei Lee (2009): H-PDLC/Clay Nanocomposites, Molecular Crystals and Liquid Crystals, 512:1, 167/[2013]-178/[2024]

To link to this article: http://dx.doi.org/10.1080/15421400903050855

Mol. Cryst. Liq. Cryst., Vol. 512, pp. 167/[2013]–178/[2024], 2009

ISSN: 1542-1406 print/1563-5287 online
DOI: 10.1080/15421400903050855

H-PDLC/Clay Nanocomposites

Yuan-Pin Huang[1], Yun-Min Chang[2], Tsung-Yen Tsai[2], and Wei Lee[3]
[1]Department of Chemical & Materials Engineering, Cheng Shiu University, Kaohsiung, Taiwan, Republic of China
[2]Department of Chemistry and Center for Nano-Technology, Chung Yuan Christian University, Chung-Li, Taiwan, Republic of China
[3]Department of Physics and Center for Nano-Technology, Chung Yuan Christian University, Chung-Li, Taiwan, Republic of China

Holographic polymer-dispersed liquid crystals (H-PDLCs) filled with layer-structured montmorillonite (MMT) clay were fabricated by wave mixing of two coherent argon-ion laser beams. The effects of MMT doping were investigated by comparing a pristine sodium-type MMT and an organophilic MMT (OMMT) via modification. In order to gain insights into the complex formation of the ternary nematic/polymer/clay nanocomposites, wide-angle X-ray diffraction experiments were carried out on pure liquid crystal, MMT clay, and clay dispersed in the liquid crystal in the mesophase as well as isotropic state. Self-diffraction experiments in the Raman–Nath regime revealed that the first-order diffraction efficiency was enhanced in the H-PDLCs consisting of pristine MMT nanoparticles and yet suppressed by the incorporation of OMMT. Holographic nature of the polymer-matrix nanocomposites was confirmed by optical polarizing microscopy. The results of this study may open up great promise held by such ternary polymer-matrix nanocomposites for photonic applications.

Keywords: holographic polymer-dispersed liquid crystals; montmorillonite clay; polymer-dispersed liquid crystals

INTRODUCTION

Polymer-dispersed liquid crystals (PDLCs) consisting of tiny phase-separated nematic liquid-crystal (LC) droplets [1,2] distributed

The authors thank H.-Y. Chen for assistance with beam alignment for the two-wave-mixing experiments and gratefully acknowledge financial support from the National Science Council under Grant Nos. NSC 94-2113-M-033-013 and NSC 95-2112-M-033-012-MY3.

Address correspondence to Wei Lee, Department of Physics, Chung Yuan Christian University, Chung-Li, Taiwan 32023, Republic of China. E-mail: wlee@cycu.edu.tw

in a rigid polymeric matrix have been realized with great interest in their electro-optical switching properties [3] for potential applications ranging from optical shutters to flexible displays [4–6]. Unlike a typical PDLC manufactured with ultraviolet exposure to induce the phase separation, an interference pattern of two coherent laser beams is employed in the fabrication of holographic polymer-dispersed liquid crystal (H-PDLC) composites. Due to the optical interference pattern, the concentration gradient is formed by the polymerization-induced phase separation. There is a distribution of droplet sizes within the LC-rich regions of an H-PDLC film, which is related to the kinetics of the phase-separation process. H-PDLCs permit the development of switchable transmissive and reflective diffractive devices [6]. On the other hand, owing to the recently rapid development of research areas involving nanoparticle suspensions in LCs, organo–inorganic LC composites have attracted considerable interest over the past decade [7–17]. In comparison with inorganic spherical particles or one-dimensional nanomaterials dispersed in LCs [7–17], colloidal platelets have received less attention [18–22]. As a matter of fact, platelet-like particles generate fewer topological defects when suspended in an LC [23]. Moreover, it has been suggested that PDLC hybridized with inorganic layered double hydroxide shows an improved diffraction efficiency compared with that of its pristine counterpart [24]. In this work, we focus on two comparative two-dimensional clay nanomaterials as dopants and report the effects of adding unmodified montmorillonite (MMT) and organophilic MMT (OMMT) via modification into the structure of H-PDLC films. Compared also are the optical and morphological properties of the methacrylate photopolymerized polymer/LC composites with and without the addition of clay into the starting monomer syrup. The results show that, although OMMT yields a better dispersion than MMT does, the addition of the organo-clay seriously interrupts the phase separation between polymer and LC, leading to a suppressed sensitivity in a holographic photopolymerization experiment. Furthermore, it is demonstrated that the optical performance the H-PDLC films containing MMT clay are superior to that of the pristine H-PDLC counterpart.

MATERIALS AND METHODS

Sample Preparation

The MMT clay used was PK-802, produced by PAI KONG Nanotechnology LTD, which is an octahedrally substituted sodium-type

montmorillonite with cation-exchange capacity of 116 meq per 100 g. It belongs to the smectite class, a natural layered 2:1 clay material with two tetrahedral sheets sandwiching a central octahedral layer. The MMT clay was used after thorough purification in the laboratory. For comparison, the organo-clay OMMT was also prepared, by a cation-exchange reaction with C11Z-CN (2-undecyl-1H-imidazole-1-propiononitrile) as a modifying agent. First, 5 g MMT clay was swollen in 100 g deionized water for 24 hours in beaker A. Next, 2.31 g C11Z-CN was dissolved in 100 g co-solvent of equal-amount deionized water and methyl alcohol in beaker B, followed by adding 1-M HCl to adjust the pH value around 3–4. 24 hours later, the solution in beaker A was added, drop by drop, into beaker B slowly. The resulting mixture was stirred vigorously for eight hours and then filtered and washed with deionized water. Finally, the OMMT was dried under vacuum at 60°C for 24 hours to remove water.

Before making the syrup ready for fabrication of composites with a polymeric matrix, some simple LC–MMT and LC–OMMT suspensions were prepared by mixing a commercially available nematic LC (E7) and clay at 70°C with ultrasonication for 2 hours, followed by injecting each colloidal suspension into a cell made of two parallel transparent indium–tin-oxide (ITO) glass substrates.

The monomer solution was prepared by mixing 0.6 g dipentaerythritol pentaacrylate (SR399, Sartomer), 0.083 g cross-linking N-vinylpyrrollidone (NVP, Aldrich), 0.005 g photo-initiator dye Rose Bengal (RB, Aldrich), 0.0053 g co-initiator N-phenylglycine (NPG, Aldrich) and 0.3 g E7. The nematic/polymer/clay nanocomposites were prepared by the addition of MMT or OMMT clay into the mixed syrup of 70% monomer and 30% LC. Various solutions were introduced into the cells each comprising two glass plates separated by 30 μm from each other. The concentrations of either clay were controlled to be 1, 3, and 5 parts per hundreds of rubber (phr) by weight. Due to the sensitivity to light, both the sample-preparation and material-mixing processes were carried out in the dark. Polymerization-induced phase separation was performed with the illumination of two mixed *p*-polarized coherent beams with identical intensities derived from an Ar^+ laser operating at 514.5 nm to fabricate the H-PDLC films.

Materials Examination

The X-ray analysis was done using an x-ray diffractometer (Philips X'pert Pro) equipped with a secondary monochromator and a Cu-tube for CuKα radiation of wavelength 1.54 Å. FT-IR spectra were taken on a spectrometer (Bio-Red FTS-7) between 4000 and 400 cm^{-1} with

reversible 64 scans. The morphology of LC–clay composites and H-PDLC–clay nanocomposites were observed under an optical polarizing microscope (Olympus BM2-UMA) equipped with a CCD color camera (Toshiba IK.637 F). A transmission electron microscope (Philips Tecnai-20) operating at 200 kV was used to examine the dispersability and morphology of the holographic nanocomposites.

RESULT AND DISCUSSION

General Characterization of LC–Clay Suspensions

The X-ray diffraction (XRD) scans of the purified MMT and OMMT during organic modification process are shown in Figure 1. It presents the layered periodicity with an interplanar d-spacing of 12.6 Å for the original MMT clay, corresponding to the (001) peak at $2\theta = 7.00^\circ$, where θ is the Bragg angle. The XRD pattern of the modified clay sample shows that the d-spacing of OMMT was swollen from 12.6 Å of the untreated MMT clay to 34.2 Å. It suggests that during the modifying process the long-chain organic C11Z-CN ammonium cations substituted sodium cations in the intragallery of MMT via the cation-exchange reaction, arranging themselves nearly perpendicular to the clay layers. This result implies the successful organic modification through intercalation due to the (001) peak shift in the XRD data. Figure 2 displays the FT-IR spectra of the pristine MMT clay, modifying agent C11Z-CN, and OMMT clay with interlayer modification. It is

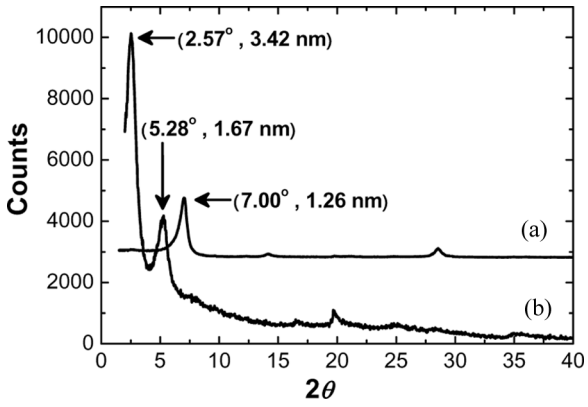

FIGURE 1 XRD patterns of (a) pristine MMT and (b) the C11Z-CN modified OMMT.

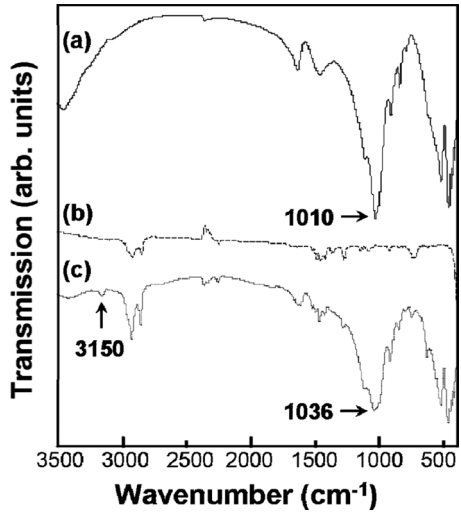

FIGURE 2 FT-IR spectra of (a) pristine MMT (b) modify agent C11Z-CN, and (c) OMMT.

clearly seen that the strong absorption band at 1010 cm^{-1} arises from in-plane Si–O–Si stretching vibrations of the pristine mineral. The strength of the same band decreases and its peak wavenumber shifts to 1036 cm^{-1} after modification with organic surfactant. In addition, the typical vibration bands of the quaternary ammonium salt (NH_4^+) detected at 3150 cm^{-1} in OMMT clay indicates that the C11Z-CN active agent was intercalated into the MMT interlayers. These results are in agreement with the finding of the expanded *d*-spacing as determined by XRD.

Figure 3 illustrates the XRD patterns of pure LC and LC–MMT suspension at various temperatures. In addition to the broad liquid-like scattering feature normally observed in the XRD profile of a typical nematic LC, pure E7 at room temperature yields a weak peak at $2\theta = 3.31^\circ$, indicating some short-range order associated with a smectic-like *d*-spacing of 26.6 Å as shown in Figure 3(a). Figures 3(b)–(e) depict the XRD patterns of 5-phr pristine MMT clay dispersed in E7 at elevated temperatures. Special attention should be paid to the signal at $2\theta = 3.31^\circ$ which increases drastically as shown in Figure 3 (b). The XRD peak declines with increasing temperature and diminishes at a temperature above the nematic-to-isotropic transition temperature ($\sim$60°C), indicating that the signal is, indeed, associated with the LC. Because of the enhanced positional order by the addition of MMT [Fig. 3(b)], we speculate that stacks of the alumosilicate platelets

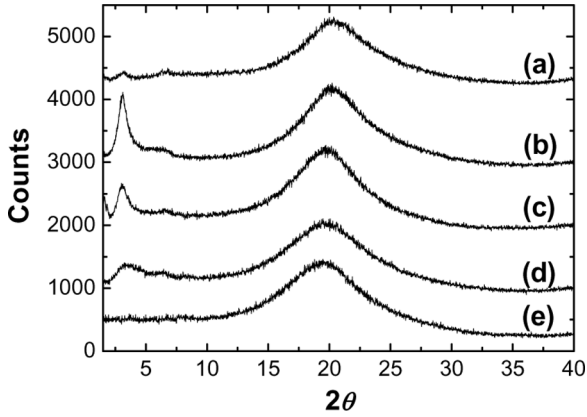

FIGURE 3 XRD patterns of (a) neat LC at 20°C and 5-phr MMT dispersed in LC at (b) 20°C, (c) 40°C, (d) 60°C, and (e) 80°C.

swelled to allow the intergallery distance to resemble the periodicity of the layer-like structure of E7. This is certainly a topic of scientific interest. Further investigations are needed.

The influence of clay as an additive on the optical properties of an LC host was examined by optical polarizing microscopy (POM) with crossed linear polarizers. Neat LC was first evaluated as the reference. The result is shown in Figure 4(a). Samples of 1 phr of clay, either MMT or OMMT, dispersed in an LC hydrosol were then investigated. Noticeably, there are some defects in the image resulting from the interaction between MMT clay and LC matrix [see Fig. 4(b)]. Nevertheless, the texture of LC dispersed with MMT clay seems similar to that of the neat LC. In contrast, the optical texture of the LC dispersed with OMMT clay, as shown in Figure 4(c), is very different from that of the others. As implied by Figure 4(c), the OMMT clay seems to blend with the LC better than its pristine counterpart, thanks to the organically modifying agent

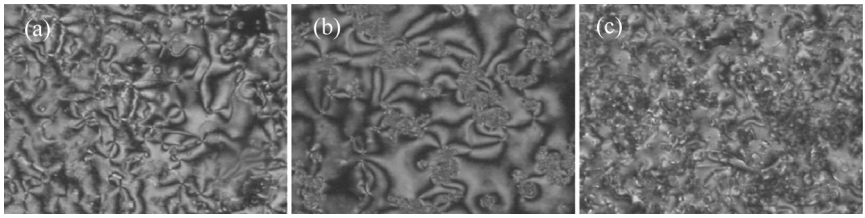

FIGURE 4 POM images of (a) neat LC, (b) 1-phr MMT dispersed in LC, and (c) 1-phr OMMT dispersed in LC.

C11Z-CN. However, as also revealed by the same figure, a lack of conspicuous birefringence indicates that the composite containing OMMT possessed a depressed anisotropy belonging to the mesophase.

H-PDLC Nanocomposites

A two-wave-mixing experiment as illustrated in Figure 5(a) was performed in order to generate the holographic grating in a sample. The two *p*-polarized writing beams of nearly equal intensity were derived from a linearly polarized cw Ar^+ laser operating at the 514.5-nm line. The sample normal was parallel to the bisector of the two beams. The wave-mixing angle was adjustable. The beam diameter was $\sim$3 mm at the intersection on the sample. Without an externally applied electric field, an efficient self-diffraction with multiple orders of self-diffraction was visible in the far field.

The intensity of the incident beams, I_1 and I_2, and the intensity of the first Raman–Nath order of self-diffraction of beam 1, I_{-1}, were measured with two identical silicon detectors and a dual-channel optical meter interfaced with a personal computer. Owing to the unavoidable light scattering from the sample, an iris diaphragm was used for each detector throughout the %experiment. The diffraction efficiency is conventionally defined as

$$\eta = \left(\frac{I_{-1}}{I_1}\right) \times 100\% \tag{1}$$

Self-diffraction efficiencies of H-PDLC transmission gratings inscribed in various nanocomposite films were investigated by measuring the intensity of the first-order diffracted beam [7,25] without a probe beam. These polymer/LC composite systems were composed of alternating regions of polymer-rich and LC-rich layers. They were made from a mixture of photosensitive prepolymer and E7 which was exposed to two interfering laser beams as previously described. Polymerization took place more rapidly in bright regions than in dark regions to allow the LC molecules to diffuse to dark regions whereas the monomer to the bright ones [26]. As a consequence, the LC droplets were formed in the dark regions. The refractive index was modulated in the planar composite due to the phase separation, giving rise to an optical phase grating.

Figure 5(b) shows the dependence of the first-order self-diffraction efficiency η of an undoped H-PDLC grating on the two-wave-mixing angle α up to 8°. It is clear that the diffraction efficiency varied with the wave-mixing angle, rose very rapidly, reached maximum at $\alpha = 2°$,

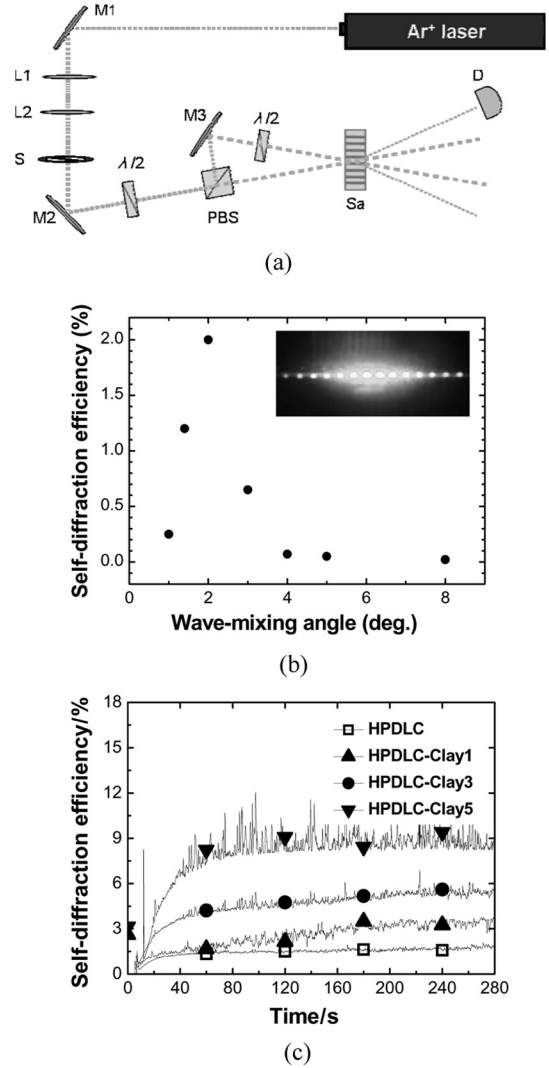

FIGURE 5 (a) Schematic illustration of the experimental geometry for holographic recording and real-time optical reading. D, detector; L1–L2, lenses; M1–M3, mirrors; PBS, polarizing beam splitter; S, shutter; Sa, sample; $\lambda/2$, half-wave plates. Both excitation-beam fluxes varied identically between 5 mW/cm^2 and 60 mW/cm^2. (b) Wave-mixing angle dependence of the first-order self-diffraction efficiency of a grating written in a pristine HPDLC with two 40-mW/cm^2 coherent beams. The Inset shows a self-diffraction pattern. (c) Temporal traces of the first-order diffraction efficiencies of a pristine HPDLC, HPDLC–MMT 1, HPDLC–MMT 3, and HPDLC–MMT 5 at 40 mW/cm^2.

and then fell afterward. In accordance with the formula

$$\Lambda = \frac{\lambda}{2\sin\left(\frac{\alpha}{2}\right)} \tag{2}$$

where $\lambda = 0.5145\,\mu m$ for the beam wavelength, this specific wave-mixing angle yielded a grating constant of $15\,\mu m$. Figure 5(c) shows the self-diffraction efficiencies as a function of time for a pristine H-PDLC grating and three doped H-PDLC–MMT counterparts containing various MMT contents (1, 3, and 5 phr) formed by two coherent beams of identical intensity of 60 mW/cm^2 at a fixed wave-mixing angle 2°. Note that, in Figure 5(c), each label for a sample carrying a numerical figure stands for the MMT content in phr. One can see from Figure 5(c) that it took minutes to get to the steady state of diffraction efficiency and all H-PDLC films embedding non-reactive MMT mineral exhibited enhanced sensitivity in comparison with the pristine H-PDLC film. Table 1 summarizes the intensity-dependent steady-state self-diffraction efficiencies for the undoped composite film and various MMT- and OMMT-doped H-PDLC gratings. It illustrates that the incorporation of MMT clay (up to 5 phr in this study) to an H-PDLC film promoted the optical diffractive properties, leading to the efficiency of up to five fold higher. On the contrary, the addition of OMMT clay caused the appearance of the cells to be translucent and suppressed the self-diffraction efficiency. The fact that the self-diffraction efficiency decreased as the content of OMMT clay increased implies that the formation of the H-PDLC grating was vital to the presence of the OMMT clay in the film.

TABLE 1 Self-diffraction efficiencies as a function of the beam intensity of a pristine H-PDLC and MMT- and OMMT-doped H-PDLCs with various clay contents

Self-diffraction efficiencies η (%)				
	Single-beam intensity			
Sample code	5 mW/cm^2	20 mW/cm^2	40 mW/cm^2	60 mW/cm^2
HPDLC	0.61	0.83	1.86	2.48
HPDLC–MMT 1	0.56	2.21	3.16	3.61
HPDLC–MMT 3	0.65	3.23	4.26	5.43
HPDLC–MMT 5	1.35	5.01	7.19	8.79
HPDLC–OMMT 1	0.55	0.25	1.51	1.14
HPDLC–OMMT 3	0.62	0.62	1.04	1.04
HPDLC–OMMT 5	0.46	0.76	0.82	0.75

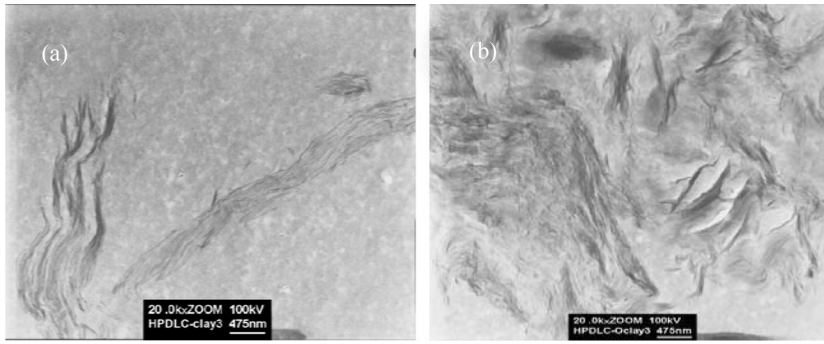

FIGURE 6 TEM images of (a) HPDLC–MMT 3 and (b) HPDLC–OMMT 3.

In order to observe the morphologies of the MMT and OMMT clay dispersed into H-PDLCs, an H-PDLC–MMT 3 sample and an H-PDLC–OMMT 3 sample were examined by transmission electron microscopy (TEM). Figure 6 displays the TEM images. It is shown that the MMT clay was dispersed in the composite, confirming the intercalated morphology [see Fig. 6(a)]. On the other hand, the OMMT clay can be seen to expand by the modifying agent C11Z-CN after organic modification process and both states of intercalation and exfoliation occurred in the H-PDLC–OMMT sample as shown in Figure 6(b). Thus, OMMT, yielding a better-dispersed nanocomposite as expected, is superior to MMT from the point of view of materials. However, the organophilicity of OMMT may have repressed the phase separation during the formation of an H-PDLC grating.

To gain further insight into the grating microstructure of the comparative 5-phr-clay-doped H-PDLC films, two representative samples

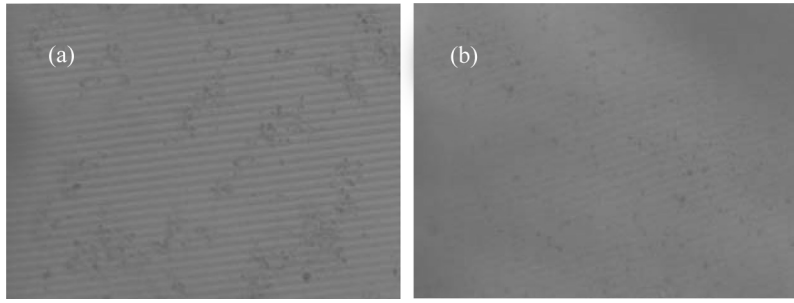

FIGURE 7 POM images of (a) HPDLC–MMT 3 and (b) HPDLC–OMMT 3 with two 20-mW/cm^2 coherent beams.

were observed directly by POM. These samples were taken out of the cells and etched with *n*-hexane to remove excess LC prior to the microscopic examination. Figures 7(a) and (b) display the POM images of the H-PDLC–MMT 5 and H-PDLC–OMMT 5 films with gratings recorded by an interference pattern of two 20-mW/cm^2 coherent beams. It is seen that the successive polymer- and LC-rich stripes resembling the interference pattern with a periodicity of $\sim$15 μm are more pronounced in the H-PDLC–MMT than the H-PDLC–OMMT sample. This result is in good agreement with the observation of the self-diffraction efficiency.

CONCLUSIONS

Colloidal clay platlets have been successfully prepared in a syrup of photosensitive prepolymer and a typical nematic liquid crystal. The optical and morphological properties of holographically formed polymer-dispersed liquid crystal composites with and without the addition of clay are described and the effects caused by the pristine clay and organically modified clay are compared. It is shown that, while the organophilic montmorillonite mineral yielded a better-dispersed nanocomposite, the grating recorded in a holographic polymer-dispersed liquid crystal composite consisting of pristine montmorillonite exhibited an enhanced self-diffraction efficiency. We realize that the diffraction efficiencies demonstrated in this study are not considered high for systems of this type and that a five-fold increase in diffraction efficiency for films with such mediocre values has limited added value. We note that many high-quality gratings in polymer-dispersed liquid crystal composites can be fabricated with the aid of an applied voltage. This preliminary work is intended to draw attention in the broad liquid-crystal community. After all, the science of polymer/liquid-crystal composites containing aspherical nanodopants alone is of great interest, indeed. Studies of electro-optical properties including the switching characteristics of the discussed nanocomposites are underway in this laboratory.

REFERENCES

[1] Drzaic, P. S. (2003). *Liquid Crystal Dispersions*, World Scientific: Singapore.
[2] Doane, J. W., Vaz, N. A., Wu, B.-G., & Žumer, S. (1986). *Appl. Phys. Lett.*, *48*, 269.
[3] Doane, J. W., Chidichimo, G., & Vaz, N. A. (1987). *US Patent*, 4,688,900.
[4] Wu, S.-T. & Yang, D. K. (2001). *Reflective Liquid Crystal Displays*, Wiley: New York.
[5] Crawford, G. P. (2005). *Flexible Flat Panel Displays*, Wiley: New York.
[6] Bunning, T. J., Natarajan, L. V., Tondiglia, V. P., & Sutherland, R. L. (2000). *Annu. Rev. Mater. Sci.*, *30*, 83.
[7] Lee, W. & Chiu, C.-S. (2001). *Opt. Lett.*, *26*, 521.

[8] Suzuki, M., Furue, H., & Kobayashi, S. (2001). *Mol. Cryst. Liq. Cryst.*, *368*, 3959.
[9] Woltman, S. J. & Crawford, G. P. (2005). *SID 05 Digest*, 752.
[10] Kaur, S., Singh, S. P., & Biradar, A. M. (2007). *Appl. Phys. Lett.*, *91*, 023120.
[11] Toko, Y., Yokoyama, S., Takigawa, S., Nishino, S., Toshima, N., & Kobayashi, S. (2007). *SID 07 Digest*, 158.
[12] Li, F., West, J., Glushchenko, A., Cheon, C. I., & Reznikov, Y. (2006). *J. Soc. Info. Display*, *14*, 523.
[13] Sano, S., Miyama, T., Takatoh, K., & Kobayashi, S. (2006). *Proc. SPIE*, *6135*, 613501.
[14] Ewiss, M. A. Z., Moawia, F., & Stoll, B. (2007). *Liq. Cryst.*, *34*, 127.
[15] Matsui, E. & Yasuda, A. (1997). *Phys. Rev. E*, *56*, 600.
[16] Williams, Y., Chan, K., Park, J. H., Khoo, I. C., Lewis, B., & Mallouk, T. E. (2005). *Proc. SPIE*, *5936*, 593613.
[17] Wu, K.-J., Chu, K.-C., Chao, C.-Y., Chen, Y.-F., Lai, C.-W., Kang, C.-C., Chen, C.-Y., & Chou. P.-T. (2007). *Nano Lett.*, *7*, 1908.
[18] Kawasumi, M., Hasegawa, N., Usuki, A., & Okada, A. (1999). *Appl. Clay Sci.*, *15*, 93.
[19] Pizzey, C., Klein, S., Leach, E., van Duijneveldt, J. S., & Richardson, R. M. (2004). *J. Phys. Condes. Matter*, *16*, 2479.
[20] Baran, J., Dolgov, L., Gavrilko, T., Osinkina, L., Puchkovska, G., Ratajczak, H., Shaydyuk, Y., & Hauser, A. (2007). *Phil. Mag.*, *87*, 4273.
[21] Chang, Y.-M., Tsai, T.-Y., Huang, Y.-P., Chen, W.-S., & Lee, W. (2007). *Jpn. J. Appl. Phys.*, *46*, 7368.
[22] Bezrodna, T., Chashechnikova, I., Gavrilk, T., Puchkovska, G., Shaydyk, Y., Tolochko, A., Baran, J., & Drozd, M. (2008). *Liq. Cryst.*, *35*, 265.
[23] Zhang, Z. & van Duijneveldt, J. S. (2007). *Soft Matter*, *3*, 596.
[24] Tsai, T.-Y., Lu, S.-W., Huang, Y.-P., & Li, F.-S. (2006). *J. Phys. Chem Solids*, *67*, 938.
[25] Huang, Y.-P., Tsai, T.-Y., Lee, W., Chin, W.-K., Chang, Y.-M., & Chen, H.-Y. (2005). *Opt. Express*, *13*, 2058.
[26] Bowley, C. C. & Crawford, G. P. (2000). *Appl. Phys. Lett.*, *76*, 2235.